ISSN 1392 - 1207. MECHANIKA. 2013 Volume 19(3): 316-323

Hybrid modeling and analysis of structural dynamic of a ball screw feed drive system

Liang Dong*, WenCheng Tang**
**School of Mechanical Engineering, Southeast University, Nanjing, China, E-mail: dl_seu@163.com*
***School of Mechanical Engineering, Southeast University, Nanjing, China, E-mail: tangwc@seu.edu.cn*

crossref http://dx.doi.org/10.5755/j01.mech.19.3.4662

1. Introduction

Ball screw drives are widely used as the motion delivery mechanism due to their high stiffness and high accuracy. As the speed and precision requirements from machine tools increase, the effects of the structural flexibility of the drives on controller performance are becoming increasingly significant. The vibrations adversely affect the positioning accuracy and performance of the drive. The natural frequencies of a ball screw system vary as the nut moves along the screw. It is necessary to have an insight into the dynamic response of the rotating ball screw subjected to axially moving load during prototyping of the machine tool and controller [1].

Conventional dynamic modeling methods of the ball screw drives employ lumped parameter models [2-4], which cannot accurately characterize the high frequency mechanical resonance. More advanced models are obtained with the help of hybrid methods that consider torsional, axial, and possibly flexural vibrations. Varanasi et al. [5] and Whally et al. [6] captured the axial and torsional dynamics of a ball screw drive using beam formulations. In general, these models cannot accurately characterize the high frequency mechanical resonances. Frey et al. [7] proposed an approach aims at identifying the dominant effects of the ball screw and including them into a simple lumped mass model. Vicente et al. [8] studied the axial and torsional coupled vibration by Ritz serious method. Finite Element methods are often incorporated in modeling the drive systems. Zhou et al. [9] presented a model only considering the axial dynamics of the screw. However, neither model considers the flexural deformation. Okwudire et al. [10] proposed a model of ball screw using beam elements having axial, torsional, and lateral dynamics.

This paper presents a hybrid model of a ball screw drive, in which the screw is considered as a Timoshenko's beam having axial，torsional and flexural dynamics. The deformation of the screw is determined by assumed mode method. The method models the dynamic behavior of a ball screw considering the moving nut. The dynamic equations of a rotating screw subjected to the axially moving load with general boundary conditions are proposed.

2. Hybrid modeling

A ball screw drive feed system proposed in this paper is shown in Fig. 1. Actuation is provided through a servomotor that is connected to the ball screw using a coupling. The screw is constrained to the machine base through a thrust bearing at the motor side.

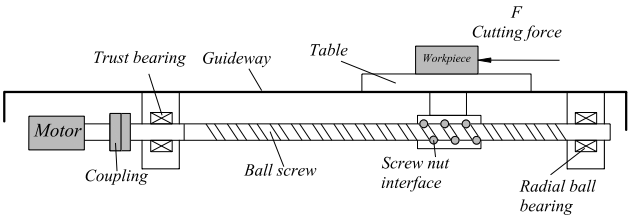

Fig. 1 Mechanical components of a ball screw feed drive

The vibration of a ball screw feed drive can be characterized by three different modes: axial, torsional and flexural as shown in Fig. 2. It should be notice that in order to keep the model complexity minimal the modeling of the nut dynamic, which have been successful modeled by Okwudire [10], is not considered in this article.

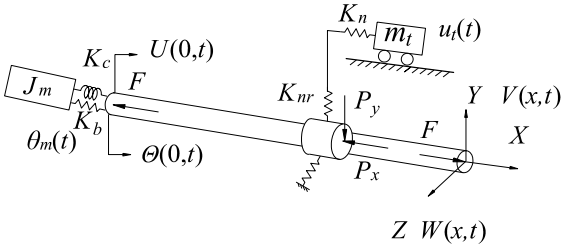

Fig. 2 Dynamic structural model of a ball screw feed drive system

The ball screw considered is an axisymmetric uniform shaft rotating about its longitudinal axis with a constant angular velocity Ω, as shown in Fig. 2. The rotating screw is subjected to two forces P_x, P_y moving along the x-axis. P_x, P_y are applied in the directions of the X and Y axes. P_x is the axial load. The mass of the ball in the nut is considered as concentrated mass expressed as P_y. F is the preload.

The screw is characterized by density ρ, cross-section A, length L, polar moment of inertia J, Young's modulus E, Poisson's modulus G, and screw pitch l.

The relatively more rigid components are represented as lumped parameters connected by springs at joint interfaces. The lumped parameters are defined by the axial stiffness K_b, the torsional stiffness K_c of the coupling, the axial stiffness K_n and radial stiffness K_{nr} of the nut, the inertia of the motor J_m and the coupling J_c, the mass of the table m_t.

2.1. Axial-torsional model

The continuous deformation of the ball screw can be represented by an axial displacement using a field func-

tion $U(x, t)$, by an angular displacement using $\Theta(x, t)$. The $u_t(t)$ and $\theta_m(t)$ each represents the displacement of the table and the angle of rotation of the motor.

$$U(x,t)=\sum_{i=1}^{N}u_i(x)\varphi_i(t);\quad \Theta(x,t)=\sum_{i=1}^{N}\theta_i(x)\eta_i(t), \tag{1}$$

where $u_i(x)$ and $\theta_i(x)$ are shape functions that satisfy the corresponding boundary conditions; $\varphi_i(t)$ and $\eta_i(t)$ are the respective modal displacements.

For the screw-nut interface, the preloaded nut serves as a special spring that couples different degrees of freedom, especially in the torsional and axial directions. The axial deformation of the screw-nut interface δ_n can be expressed as:

$$\delta_n=U_t(t)-\left[U(x_t,t)+\Theta(x_t,t)\frac{l}{2\pi}\right]. \tag{2}$$

The kinetic energy T of the axial-torsional coupled system, due to the distributed inertia of the screw, the mass of the table, the inertia of the rotor and the energy from the flexible coupling, can be computed as:

$$T=\frac{1}{2}\rho A\int_0^L\dot{U}(x,t)^2dx+\frac{1}{2}\rho J\int_0^L\dot{\Theta}(x,t)^2dx+$$
$$+\frac{1}{2}m_t\dot{u}_t(t)^2+\frac{1}{2}J_m\dot{\theta}_m(t)^2+\frac{1}{2}J_c\left(\frac{\dot{\theta}_m(t)+\dot{\Theta}(0,t)}{2}\right)^2, \tag{3}$$

where the symbols $(\cdot)$ denotes differentiation with respect to time.

The potential energy U, due to the potential energy stored in the elastic parts including the screw , coupling, screw nut interface and preload, is defined as:

$$U=\frac{1}{2}EA\int_0^L U'(x,t)^2dx+\frac{1}{2}GJ\int_0^L\Theta'(x,t)^2dx+$$
$$+\frac{1}{2}K_bU(0,t)^2+\frac{1}{2}K_n\delta_n{}^2+$$
$$+\frac{1}{2}K_c\left[\theta_m(t)-\Theta(0,t)\right]^2+\frac{1}{2}F\int_0^L U'(x,t)^2dx\ , \tag{4}$$

where the symbols " $'$ " indicate differentiation with respect to x.

Define:

$$\left.\begin{array}{l}\boldsymbol{\varphi}=\{\varphi_1,\varphi_2...,\varphi_n\}^T;\ \boldsymbol{\eta}=\{\eta_1,\eta_2...,\eta_n\}^T;(\boldsymbol{M})_{ij}=\int_0^L u_iu_jdx;(\boldsymbol{S})_{ij}=\int_0^L\theta_i\theta_jdx;(\boldsymbol{K})_{ij}=\theta_i(x=0)\theta_j(x=0);\\ (\boldsymbol{Y})_{ij}=\theta_i(x=x_t)\theta_j(x=x_t);(\boldsymbol{R})_{ij}=\int_0^L u_i'u_j'dx;(\boldsymbol{U})_{ij}=\int_0^L\theta_i'\theta_j'dx;(\boldsymbol{W})_{ij}=u_i(x=0)u_j(x=0);\\ (\boldsymbol{V})_{ij}=u_i(x=x_t)u_j(x=x_t);(\boldsymbol{Z})_{ij}=u_i(x=x_t)\theta_j(x=x_t);(\boldsymbol{Y})_{ij}=\theta_i(x=x_t)\theta_j(x=x_t);(\boldsymbol{X})_{ij}=\theta_i(x=0)\theta_j(x=0);\\ (\boldsymbol{Q})_{ij}=\theta_i(x=L)\theta_j(x=L);(\boldsymbol{a}_{N\times1})_i=u_i(x=x_t);(\boldsymbol{b}_{1\times N})_i=\theta_i(x=x_t);(\boldsymbol{c}_{1\times N})_i=\theta_i(x=0);\ i=1,2,...,N;\quad j=1,2,...,N.\end{array}\right\} \tag{5}$$

The energy can be expressed in matrix form:

$$T=\frac{1}{2}\rho A\dot{\boldsymbol{\varphi}}^T\boldsymbol{M}\dot{\boldsymbol{\varphi}}+\frac{1}{2}\rho J\dot{\boldsymbol{\eta}}^T\boldsymbol{S}\dot{\boldsymbol{\eta}}+\frac{1}{2}m_t\dot{u}_t(t)^2+$$
$$+\frac{1}{2}\left(J_m+\frac{1}{4}J_c\right)\dot{\theta}_m(t)^2+\frac{1}{4}J_c\dot{\theta}_m(t)\boldsymbol{c}\dot{\boldsymbol{\eta}}+$$
$$+\frac{1}{8}J_c\dot{\boldsymbol{\eta}}^T\boldsymbol{K}\dot{\boldsymbol{\eta}}\ ; \tag{6}$$

$$U=\frac{1}{2}EA\boldsymbol{\varphi}^T\boldsymbol{R}\boldsymbol{\varphi}+\frac{1}{2}GJ\boldsymbol{\eta}^T\boldsymbol{U}\boldsymbol{\eta}+\frac{1}{2}K_b\boldsymbol{\varphi}^T\boldsymbol{W}\boldsymbol{\varphi}+$$
$$+\frac{1}{2}K_n\left[\begin{array}{l}u_t(t)^2-2u_t(t)\boldsymbol{a}\boldsymbol{\varphi}-\frac{l}{\pi}u_t(t)\boldsymbol{b}\boldsymbol{\eta}+\\ \boldsymbol{\varphi}^T\boldsymbol{V}\boldsymbol{\varphi}+\frac{l}{\pi}\boldsymbol{\varphi}^T\boldsymbol{Z}\boldsymbol{\eta}+\left(\frac{l}{2\pi}\right)^2\boldsymbol{\eta}^T\boldsymbol{Y}\boldsymbol{\eta}\end{array}\right]+$$
$$+\frac{1}{2}K_c\left[\theta_m(t)^2-2\theta_m(t)\boldsymbol{c}\boldsymbol{\eta}+\boldsymbol{\eta}^T\boldsymbol{X}\boldsymbol{\eta}\right]+\frac{1}{2}F\boldsymbol{\varphi}^T\boldsymbol{R}\boldsymbol{\varphi}\ . \tag{7}$$

The work done due to the moving load P_x is $\delta W=P_x\delta U(x_t,t)$. Through Lagrangian approach, the equations of motion for the system is given as:

$$\left.\begin{array}{l}\rho A\boldsymbol{M}\ddot{\boldsymbol{\varphi}}+\left(EA\boldsymbol{R}+K_b\boldsymbol{W}+K_n\boldsymbol{V}+F\boldsymbol{R}\right)\boldsymbol{\varphi}-\\ -K_n\boldsymbol{a}^Tu_t+\frac{l}{2\pi}K_n\boldsymbol{Z}^T\boldsymbol{\eta}=P_x\boldsymbol{a};\\ m_t\ddot{u}_t+K_nu_t-K_n\boldsymbol{a}\boldsymbol{\varphi}-\frac{l}{2\pi}K_n\boldsymbol{b}\boldsymbol{\eta}=0;\\ \left(\rho J\boldsymbol{S}+\frac{1}{4}J_c\boldsymbol{K}\right)\ddot{\boldsymbol{\eta}}+\frac{1}{4}J_c\boldsymbol{c}^T\ddot{\theta}_m+\\ +\left(GJ\boldsymbol{U}+\left(\frac{l}{2\pi}\right)^2K_n\boldsymbol{Y}+K_c\boldsymbol{X}\right)\boldsymbol{\eta}+\\ +\frac{l}{2\pi}K_n\boldsymbol{Z}^T\boldsymbol{\varphi}-\frac{l}{2\pi}K_n\boldsymbol{b}^Tu_t-K_c\boldsymbol{c}^T\boldsymbol{\theta_m}=0;\\ \left(J_m+\frac{1}{4}J_c\right)\ddot{\theta}_m+\frac{1}{4}J_c\boldsymbol{c}\ddot{\boldsymbol{\eta}}+K_c\theta_m-K_c\boldsymbol{c}\boldsymbol{\eta}=0,\end{array}\right\} \tag{8}$$

where the preload F can enhance the axial stiffness of the whole system.

2.2. Flexural model

Based on Timoshenko's beam theory, the deformed screw can be described by the transverse translations $V(x, t)$ and $W(x, t)$ in Y and Z directions and small rotations $B(x, t)$ and $\Gamma(x, t)$ about the Y and Z, respectively. The translations V, W consist of a contribution V_b, W_b due

to bending and a contribution V_s, W_s due to transverse shear deformation. The relations among these variables are:

$$\left.\begin{aligned} &V(x,t)=V_b(x,t)+V_s(x,t);\\ &W(x,t)=W_b(x,t)+W_s(x,t);\\ &B(x,t)=-\partial W_b(x,t)/\partial x;\\ &\Gamma(x,t)=\partial V_b(x,t)/\partial x. \end{aligned}\right\} \tag{9}$$

Using the assumed mode method, V, W, Γ, B can be expressed:

$$V(x,t)=\sum_{i=1}^{n} v_i(t)\phi_i(x);\quad W(x,t)=\sum_{i=1}^{n} w_i(t)\phi_i(x);$$
$$B(x,t)=\sum_{i=1}^{n} p_i(t)\psi_i(x);\quad \Gamma(x,t)=\sum_{i=1}^{n} q_i(t)\psi_i(x), \tag{10}$$

where $\phi_i(x)$ and $\psi_i(x)$ are shape functions that satisfy the corresponding boundary conditions; $v_i(t)$, $w_i(t)$, $p_i(t)$ and $q_i(t)$ are the respective modal displacements.

The kinetic energy T_f, due to the screw rotating at a constant speed Ω:

$$\begin{aligned} T_f=&\frac{1}{2}\int_0^L \rho A\left\{\dot V^2+\dot W^2\right\}dx+\frac{1}{2}\int_0^L I_d\left\{\dot\Gamma^2+\dot B^2\right\}dx-\\ &-\frac{1}{2}\Omega I_p\int_0^L\left\{\dot\Gamma B-\dot B\Gamma\right\}dx+\frac{1}{2}\Omega^2\int_0^L I_p dx, \end{aligned} \tag{11}$$

where $I=\pi r^4/4$, $I_d=\rho I$ and $I_p=2\rho I$ are the diametral and polar mass moments of inertia of the shaft per unit length.

The kinetic energy T_M, due to moving mass[11]:

$$T_M=\frac{1}{2}m_b\left[\begin{aligned} &v_m{}^2+\left(\frac{\partial V}{\partial t}+v_m\frac{\partial V}{\partial x}\right)^2+\\ &+\left(\frac{\partial W}{\partial t}+v_m\frac{\partial W}{\partial x}\right)^2 \end{aligned}\right]_{x=v_m t}. \tag{12}$$

The potential energy U_f, due to shear deformation and elastic bending, the preload F and moving axial force P_x is:

$$\begin{aligned} U_f=&\frac{1}{2}\int_0^L EI\left\{\left(V_b''\right)^2+\left(W_b''\right)^2\right\}dx+\\ &+\frac{1}{2}\int_0^L \kappa GA\left\{\left(V_s'\right)^2+\left(W_s'\right)^2\right\}dx-\\ &-\frac{1}{2}P_x\int_s^L\left\{\left(V'\right)^2+\left(W'\right)^2\right\}dx+\\ &+\frac{1}{2}F\int_0^L\left\{\left(V'\right)^2+\left(W'\right)^2\right\}dx+\\ &+\frac{1}{2}K_{nr}\left(V(x_t,t)^2+W(x_t,t)^2\right), \end{aligned} \tag{13}$$

where κ is the shear coefficient.

Define:

$$\left.\begin{aligned} &\left(\hat{\boldsymbol M}\right)_{ij}=\int_0^L\phi_i\phi_j dx;\quad \left(\hat{\boldsymbol S}\right)_{ij}=\int_0^L\psi_i\psi_j dx;\quad \left(\hat{\boldsymbol K}\right)_{ij}=\int_0^L\psi_i'\psi_j' dx;\quad \left(\hat{\boldsymbol E}\right)_{ij}=\int_0^L\psi_i\phi_j' dx;\quad \left(\hat{\boldsymbol H}\right)_{ij}=\int_0^L\phi_i'\phi_j' dx;\\ &\left(\hat{\boldsymbol G}_{\boldsymbol s}\right)_{ij}=\int_{s(t)}^L\phi_i'\phi_j' dx;\quad \left(\hat{\boldsymbol C}\right)_{ij}=\phi_i'\left(x=v_m t\right)\phi_j'\left(x=v_m t\right);\quad \left(\hat{\boldsymbol B}\right)_{ij}=\phi_i\left(x=v_m t\right)\phi_j\left(x=v_m t\right);\\ &\left(\hat{\boldsymbol A}\right)_{ij}=\phi_i\left(x=v_m t\right)\phi_j'\left(x=v_m t\right)-\phi_i'\left(x=v_m t\right)\phi_j\left(x=v_m t\right);\quad \left(\hat{\boldsymbol c}_{n\times 1}\right)_i=\phi_i\left(x=s(t)\right);\ i=1,2,...,n;\ j=1,2,...,n. \end{aligned}\right\} \tag{14}$$

The energy can be expressed in matrix form as:

$$T_f=\frac{1}{2}\rho A\dot{\boldsymbol v}^T\hat{\boldsymbol M}\dot{\boldsymbol v}+\frac{1}{2}\rho A\dot{\boldsymbol w}^T\hat{\boldsymbol M}\dot{\boldsymbol w}+\frac{1}{2}I_d\dot{\boldsymbol p}^T\hat{\boldsymbol S}\dot{\boldsymbol p}+\frac{1}{2}I_d\dot{\boldsymbol q}^T\hat{\boldsymbol S}\dot{\boldsymbol q}-\frac{1}{2}I_p\Omega\dot{\boldsymbol q}^T\hat{\boldsymbol S}\boldsymbol p+\frac{1}{2}I_p\Omega\dot{\boldsymbol p}^T\hat{\boldsymbol S}\boldsymbol q+\frac{1}{2}\Omega^2\int_0^L I_p dx; \tag{15}$$

$$\begin{aligned} U_f=&\frac{1}{2}EI\boldsymbol p^T\hat{\boldsymbol K}\boldsymbol p+\frac{1}{2}EI\boldsymbol q^T\hat{\boldsymbol K}\boldsymbol q+\frac{1}{2}\kappa GA\boldsymbol v^T\hat{\boldsymbol H}\boldsymbol v+\frac{1}{2}\kappa GA\boldsymbol w^T\hat{\boldsymbol H}\boldsymbol w+\frac{1}{2}\kappa GA\boldsymbol p^T\hat{\boldsymbol S}\boldsymbol p+\frac{1}{2}\kappa GA\boldsymbol q^T\hat{\boldsymbol S}\boldsymbol q-\kappa GA\boldsymbol q^T\hat{\boldsymbol E}\boldsymbol v+\\ &+\kappa GA\boldsymbol p^T\hat{\boldsymbol E}\boldsymbol w-\frac{1}{2}P_x\boldsymbol v^T\hat{\boldsymbol G}_{\boldsymbol s}\boldsymbol v-\frac{1}{2}P_x\boldsymbol w^T\hat{\boldsymbol G}_{\boldsymbol s}\boldsymbol w+\frac{1}{2}F\boldsymbol v^T\hat{\boldsymbol H}\boldsymbol v+\frac{1}{2}F\boldsymbol w^T\hat{\boldsymbol H}\boldsymbol w+\frac{1}{2}K_{nr}\boldsymbol v^T\hat{\boldsymbol B}\boldsymbol v+\frac{1}{2}K_{nr}\boldsymbol w^T\hat{\boldsymbol B}\boldsymbol w; \end{aligned} \tag{16}$$

$$T_M=\frac{1}{2}m_b v_m{}^2+\frac{1}{2}m_b\dot{\boldsymbol v}^T\hat{\boldsymbol B}\dot{\boldsymbol v}+m_b v_m\sum_i\sum_j\dot v_i\phi_i v_j\phi_j'+\frac{1}{2}m_b v_m{}^2\boldsymbol v^T\hat{\boldsymbol C}\boldsymbol v+\frac{1}{2}m_b\dot{\boldsymbol w}^T\hat{\boldsymbol B}\dot{\boldsymbol w}+m_b v_m\sum_i\sum_j\dot w_i\phi_i w_j\phi_j'+\frac{1}{2}m_b v_m{}^2\boldsymbol w^T\hat{\boldsymbol C}\boldsymbol w. \tag{17}$$

The virtual work $\delta W=m_b g\delta V(x_t,t)$. The equations described the rotating screw subjected to the axially moving load can be expressed as:

$$\left.\begin{aligned} &\left(\rho A\hat{\boldsymbol M}+m_b\hat{\boldsymbol B}\right)\ddot{\boldsymbol v}+m_b v_m\hat{\boldsymbol A}\dot{\boldsymbol v}+\left(\kappa GA\hat{\boldsymbol H}+F\hat{\boldsymbol H}-m_b v_m{}^2\hat{\boldsymbol C}-P_x\hat{\boldsymbol G}_s(s)+K_{nr}\hat{\boldsymbol B}\right)\boldsymbol v-\kappa GA\hat{\boldsymbol E}^{\boldsymbol T}\boldsymbol q+F\hat{\boldsymbol H}\boldsymbol v=m_b g\hat{\boldsymbol c};\\ &\left(\rho A\hat{\boldsymbol M}+m_b\hat{\boldsymbol B}\right)\ddot{\boldsymbol w}+m_b v_m\hat{\boldsymbol A}\dot{\boldsymbol w}+\left(\kappa GA\hat{\boldsymbol H}+F\hat{\boldsymbol H}-m_b v_m{}^2\hat{\boldsymbol C}-P_x\hat{\boldsymbol G}_s(s)+K_{nr}\hat{\boldsymbol B}\right)\boldsymbol w+\kappa GA\hat{\boldsymbol E}^{\boldsymbol T}\boldsymbol p+F\hat{\boldsymbol H}\boldsymbol w=0;\\ &I_d\hat{\boldsymbol S}\ddot{\boldsymbol p}+\Omega I_p\hat{\boldsymbol S}\dot{\boldsymbol q}+EI\hat{\boldsymbol K}\boldsymbol p+\kappa GA\hat{\boldsymbol S}\boldsymbol p+\kappa GA\hat{\boldsymbol E}\boldsymbol w=0;\\ &I_d\hat{\boldsymbol S}\ddot{\boldsymbol q}-\Omega I_p\hat{\boldsymbol S}\dot{\boldsymbol p}+EI\hat{\boldsymbol K}\boldsymbol q+\kappa GA\hat{\boldsymbol S}\boldsymbol q-\kappa GA\hat{\boldsymbol E}\boldsymbol v=0, \end{aligned}\right\} \tag{18}$$

where a time-dependent stiffness term generated by the moving axial force P_x reduces (when compressive) or increases (when tensile) the overall stiffness of the ball screw drive system.

2.3. Shape functions for general boundary conditions

For axial-torsional model, the shape functions are

$$u_i(x)=\cos\left[\frac{(i-1)\pi x}{L}\right],\ \theta_i(x)=\cos\left[\frac{(i-1)\pi x}{L}\right]. \quad (19)$$

For flexural model, three general geometric boundaries of a screw are introduced, including Clamped-Hinged (C-H), Clamped-Clamped (C-C), Hinged-Hinged （H-H). The corresponding shape functions are shown in Table 1.

Table 1

Flexural shape functions for variable boundary condition

	Boundary	Shape function
C-H	$V(0,t)=V(L,t)=0$ $W(0,t)=W(L,t)=0$ $V'(0,t)=B'(L,t)=0$ $W'(0,t)=\Gamma'(L,t)=0$	$\phi_i(x)=\frac{x}{L}\sin\left(\frac{i\pi x}{L}\right)$ $\psi_i(x)=\cos\left(\frac{i\pi x}{L}\right)$
C-C	$V(0,t)=V(L,t)=0$ $W(0,t)=W(L,t)=0$ $V'(0,t)=V'(L,t)=0$ $W'(0,t)=W'(L,t)=0$	$\phi_j=\frac{x}{L}\left(1-\frac{x}{L}\right)\sin\left(\frac{j\pi x}{L}\right)$ $\psi_i(x)=\cos\left(\frac{i\pi x}{L}\right)$
H-H	$V(0,t)=V(L,t)=0$ $W(0,t)=W(L,t)=0$ $B'(0,t)=B'(L,t)=0$ $\Gamma'(0,t)=\Gamma'(L,t)=0$	$\phi_j=\sqrt{2}\sin\left(\frac{j\pi x}{L}\right)$ $\psi_i(x)=\sqrt{2}\cos\left(\frac{i\pi x}{L}\right)$

2.4. Model verification

Eqs. (8) and (18) can be expressed as:

$$\boldsymbol{M}(t)\ddot{\boldsymbol{q}}+\boldsymbol{C}(t)\dot{\boldsymbol{q}}+\boldsymbol{K}(t)\boldsymbol{q}=\boldsymbol{F}(t), \quad (20)$$

where $\boldsymbol{M}$, $\boldsymbol{C}$ and $\boldsymbol{K}$ are the inertia, damping, and stiffness matrices, respectively. The matrices are dependent of the time, and needs to be updated as the nut moving over the screw. The $\boldsymbol{F}$ includes the generalized forces and $\boldsymbol{q}$ is the generalized vector. Eq. (20) can be solved by a Runge-Kutta method to obtain the dynamic response of the rotating ball screw under the moving load. The vibration modes can also be obtained through the characteristic equation. It is observed that the first three modes present a favorable approximation using $N=4$ terms in axial-torsional subsystem and $n=10$ terms in flexural subsystem.

In this section, measurements are made on a ball screw drive. The test bed shown in Fig. 3 moves a carriage of mass 50 kg. The parameters are listed in Table 2. The axial vibration is measured between an impact force(PCB/086C03) applied at the table (in the direction of motion of table) and axial acceleration measurements obtained from the table using accelerometer(PCB/356A32). The flexural vibration is measured using an accelerometer at each of 12 points on the screw. To investigate the variation as the table moves along the screw, each of the tests is measured at four distinct position of the table within its travel range.

Fig. 3 Ball screw drive setup

The predicted and measured resonance frequencies are listed in Table 3. It can be concluded that the predicted results have a good agreement with the measured ones. The deviation may due to the inaccuracies or ignorance in various stiffness and inertias. The axial and flexural mode shapes are shown in Fig. 4.

Table 2

Parameters of the ball screw drive system

Symbol	Value	Unit
m_t	50	kg
d	50	mm
l	25	mm
J_m	1.2e^{-3}	kg m^2
J_c	1.12e^{-3}	kg m^2
K_c	13752	N m/rad
K_t	6.5e^7	N/m
K_{nr}	1.5e^9	N/m
K_n	2.5e^9	N/m
L	1480	mm

Table 3

Predicted and measured resonance frequencies

Position (x_t, mm)	Axial Hz		Flexural Hz	
	Pre.	Mea.	Pre.	Mea.
400	138	142	130	125
600	136	137	185	189
800	135	135	187	171
1000	133	134	136	117

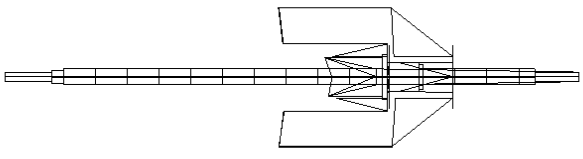

a

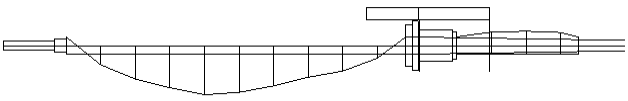

b

Fig. 4 The measured mode shapes for the ball screw drive at x_t = 1000 mm a) axial; b) flexural

Table 4

Critical rotational speed r = 0.01 m, L = 1 m

Boundary	Theoretical result, Hz	Proposed model, Hz
clamped-hinged	63.0	66.2
calmped-clamped	91.4	96.6
hinged-hinged	40.3	40.3

For different boundary conditions , the critical rotational speed is $\omega = \left(\lambda^2 / L^2\right)\sqrt{EI/\rho A}$, where λ = 3.927, 4.73, π for clamped-hinged, clamped-clamped and simply supported, respectively. Table 4 shows the critical rotational speed of a circular shaft for corresponding boundary condition. The flexural model for general boundary conditions shows a reasonable approximation for the critical rotational speed.

3. Numerical simulation and analysis

Table 5 gives the parameters used in simulation. Due to the table moves along the screw reducing the number of available measurement or excitation locations, it is impractical to measure the complex mode shapes of the ball screw assembly. Hence, the model presented here is instrumental in understanding the behavior of these modes.

Table 5

Parameters of the ball screw drive system for simulation

Symbol	Value	Unit
E	$2.06e^{11}$	N/m^2
G	$8.1e^{10}$	N/m^2
ρ	7850	kg/m^3
A	$1.1341e^{-3}$	m^2
J_c	$6.5e^{-4}$	kg m^2
J_m	$6.4e^{-3}$	kg m^2
K_b	$2.5e^{8}$	N/m
K_c	$1.41e^{5}$	Nm/rad
K_{nr}	$6e^{7}$	N/m
K_n	$5e^{8}$	N/m
L	2000	mm

3.1. Mode shapes for variable table positions

The ball screw feed drive is always subjected to a moving mass during the operation. The Fig. 5 illustrates the axial and torsional components of the mode shapes. The axial displacement of the table is described as a point value plotted at $x = x_t$. Similarly, the torsional displacement of the motor rotor is plotted at x = 0.

In Mode 1, the angular component has the smallest value compared to the other three torsional components. In addition, the displacement of the table has the largest value, which indicates that the first mode is described as an axial mode with lightly coupled with the torsional mode. The mode shape is similar with the experimental results shown in Fig. 4, a. The axial deformation of screw increases from the thrust bearing to the table position, while the value of axial deformation remains constant from table position to the right end of the screw.

In Mode 2, the amplitude of the torsional component increases considerably, whereas the axial component decreases. The axial displacement of the table is very small. Fig. 5, b shows the neural position of the torsional mode is near the motor. The torsional displacement gradually increases from left to right along the ball screw and the maximum deflection happens at the free end. The motor has a negative displacement in this mode. It can be concluded that this is a torsional predominant mode.

Finally, in Mode 3, the amplitude of the axial component shows the largest values, whereas the torsional component amplitude is also very large. There are two neutral positions in this torsional mode, one near the motor and the other between the table position and the free end. It is observed that in this mode exists a strong coupling between the axial and torsional deformation.

The variable table position almost has no influence on the torsional mode shapes, however, it has large influence on the axial mode shapes. It is obvious that the largest torsional deformation always appears at the right side of the ball screw. The mode shapes of the system provide a useful guideline for measurement.

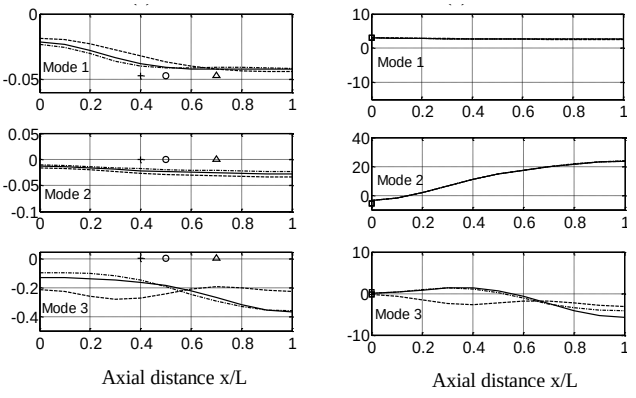

a b

Fig. 5 Axial and torsional mode shapes for l = 10 mm, m_t = 400 kg; △----: $x_t = 0.7L$; ○—:$x_t = 0.5L$; + -.-.: $x_t = 0.4L$; a) axial ; b) torsional

Fig. 6 shows the first flexural mode shapes for variable table position. Comparison of the predicted and measured mode shapes (Fig. 4, b) indicates that the flexural model can accurately describe the mode shapes of the ball screw drive. As can be expected, the variable table position has a great influence on the flexural mode shapes. Due to the table is properly amounted to the rigid guideway, and the excitation on the flexural direction is considerably small, hence the flexural modes only have tiny influence on the feed motion controller and therefore will be neglected in the following discussion. However, the flexural nature frequency of the screw is the key point for determining the critical rotational speed.

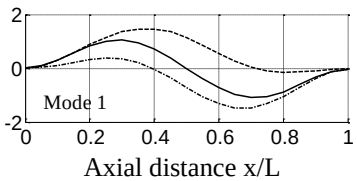

Fig. 6 Flexural mode shapes for l = 10 mm, m_t = 400 kg ----: $x_t = 0.7L$; —:$x_t = 0.5L$; -.-.: $x_t = 0.4L$

3.2. Analysis of vibration for variable operating conditions

From the controller design standpoint, it is of interest to know varies in the axial and torsional vibration according to variable operating conditions. Numerical results have been divided into three sections to investigate the effects of variable mass, screw pitch and table position, respectively. The simulation results are listed in Table 6. The first axial mode has a wide variation in resonance frequency as a function of the table position and table mass; it presents low sensitivity to the variable mass for high transmission ratio. The second mode seems almost independent of the table position and mass, which is due to the weaker stiffness coupling provided by the screw-nut interface in torsional direction. On the other hand, the third mode shows very low sensitive to the table mass, however, it presents a considerable shift for variable table position, due to its highly axial-torsional coupling.

Table 6

Simulation results of the hybrid model for variable mass, screw pitch and table position

No.	Table mass, kg	Screw pitch, mm	Table position, mm	Mode 1, Hz	Mode 2, Hz	Mode 3, Hz
1	400	10	500	97.227	466.178	704.749
2	400	10	1000	83.489	466.155	916.005
3	400	10	1500	76.509	466.139	964.433
4	400	30	500	124.415	466.147	697.950
5	400	30	1000	105.061	465.951	907.272
6	400	30	1500	95.325	465.832	990.237
7	800	10	500	72.212	466.178	701.031
8	800	10	1000	61.980	466.155	911.243
9	800	10	1500	56.759	466.139	960.445
10	800	30	500	107.308	466.147	694.502
11	800	30	1000	90.561	465.951	903.292
12	800	30	1500	82.112	465.832	986.680

Due to the stiffness of the screw decreases with increasing effective length(from the fixed bearing location to the table position), the first mode frequency decreases steadily as the table moves away from the motor while the table's vibration amplitude follows the reverse pattern. Therefore, the first axial mode can be explained by a spring mass system: the higher the mass and the greater the distance between machine table and fixed bearing the smaller the value of the first eigenfrequency. The first axial mode, due to its sensitive to the table position and mass, plays an important role in controller design and performance simulation based on the feed drive model.

The interaction between axial and torsional modes in Eq. (2) is determined by the transmission ratio of the ball screw. As can be seen from Table 6, with the increasing screw pitch the first mode frequency reveals a general trend of increase while the second and third frequencies decrease insignificantly. It indicates that the axial-torsional coupling has a great influence on the first mode frequency. The effects of the axial-torsional coupling forbid the axial and torsional mode to be considered separately, especially in high transmission ratio.

3.3. Analysis of ball screw preload variation

The nominal life of the ball screw can be calculated by an equation using the values for the basic dynamic load rating C_a and applied axial load F_{ma}:

$$T = \left(\frac{C_a}{f_w F_{ma}} \right)^3 10^6 , \tag{21}$$

where f_w is the load factor, F_{ma}, calculated by the overall applied external forces F and preload force F_{pr}, is defined as:

$$F_{ma} = F_{pr} \left(1 + \frac{F}{3F_{pr}} \right)^{3/2} . \tag{22}$$

The stiffness value of the nut K_n is obtained from the preload and elastic displacement under a preload of 10% of the basic dynamic loading rating C_a. If the preload F_{pr} is differs from $0.1C_a$, the stiffness K_n can be expressed using the following equation [12]:

$$K_n = 0.8K' \left(\frac{F_{pr}}{0.1C_a} \right)^{1/3} , \tag{23}$$

where K' is the rigidity value in the specification table.

Table 7

The first three frequencies shift for variable preload for $x_t = L/2$, $m_t = 400$ kg

F_{pr} / C_a	Mode 1, Hz	Mode 2, Hz	Mode 3, Hz
0.5%	38.17	466.15	503.36
2%	62.41	466.15	605.01
4%	73.38	466.15	710.40
8%	81.52	466.16	860.59
10%	83.49	466.16	916.01

Due to friction, lubrication and machining condition the preload will gradually decrease, which reduces the life expectancy of the ball screw. In order to examine the effect of preload variation, the first three eigenfrequencies

for variable preload are calculated in Table 7. It indicates that the first and third mode frequencies exhibit a large variation with the preload variation in the range of 0.5-10%, while the second mode frequency has no significant deviation. The first and third mode frequencies reveal a decreasing tread as the preload steps down. It can be concluded that the stiffness of the nut is of great importance on the axial mode. The simulated result has a good accordance with the experimental measurement in [4]. Therefore, the preload level can be predicted by monitoring the measured vibration dynamics, and then the life expectancy and the running status of a ball screw can be estimated.

4. Servo-control model

The servo controller should compensate for the vibration of the system and be designed carefully for any variations in the dynamics of the system [13, 14]. The hybrid model of the ball screw drive can be implemented into servo control algorithms, and then the effectiveness of various servo control algorithms can be evaluated to achieve high bandwidth control during the draft design stage of a machine.

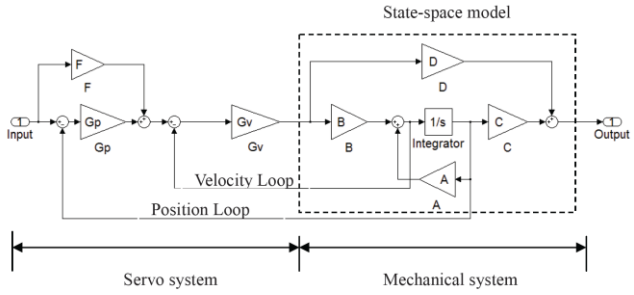

Fig. 7 Servo control system

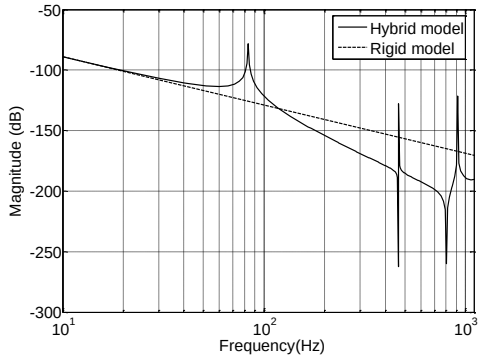

Fig. 8 Frequency response for the rigid and hybrid model

A typical servo control system is composed of the drive mechanism and the servo system, as shown in Fig. 7. In control engineering, the state space model for the mechanical model is preferred above other representations. There are a proportional controller Gp in the position loop and a proportional and integral controller Gv in the velocity loop. The velocity feedforward controller F is used to improve tracking performance.

The frequency response of hybrid and rigid model is shown in Fig. 8，it can be seen that the hybrid model captures the dynamics of the ball screw feed drives.

It is of interest to investigate the influence of the structural vibrations on the controller performance, particular the axial and torsional modes. Fig. 9 shows that due to the structural dynamics at 83 and 466 Hz, instead of obtaining a GM (Gain Margin) of 41.7 dB as indicated in rigid model, a GM of 3.67 dB is observed. In order to improve the performance of the controller, two common methods can be used: increasing the natural frequencies by the mechanical modification at the design stage and notch filtering of the structural modes of interest.

5. Conclusion

This paper has presented a hybrid dynamic model for a rotating ball screw drive subjected to axially moving load. The simulated results show a good accordance with the experimental data. Results of numerical simulations have been presented for various combinations of operation conditions. The proposed hybrid model can accurately capture the dynamic of the ball screw drive and be implemented into the design of the servo system.

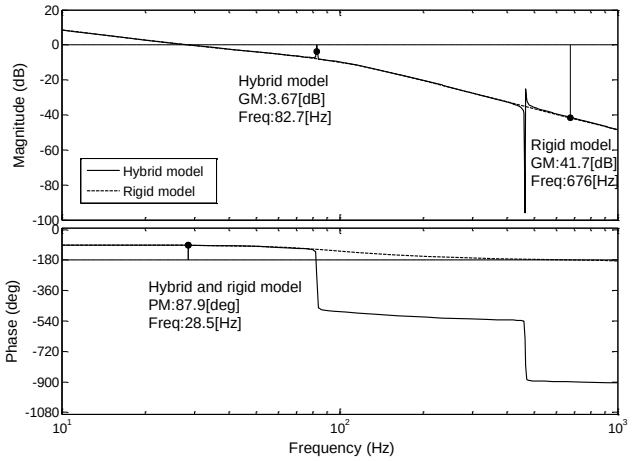

Fig. 9 Open loop bode diagram for position loop

Acknowledgment

The authors gratefully acknowledge the supports of National Science and Technology Key Projects under Grant No. 2012ZX04002-012.

References

1. **Altintas, Y.; Verl, A.; Brecher, C.; Uriarte, L.; Pritschow, G.** 2011. Machine tool feed drives, CIRP Annals - Manufacturing Technology 60(2): 779-796.
2. **Kim, M.-S.; Chung, S.-C.** 2005. A systematic approach to design high-performance feed drive systems, International Journal of Machine Tools and Manufacture 45(12-13): 1421-1435. http://dx.doi.org/10.1016/j.ijmachtools.2005.01.032.
3. **Chen, J.S.; Huang, Y.K.; Cheng, C.C.** 2004. Mechanical model and contouring analysis of high-speed ball-screw drive systems with compliance effect, The International Journal of Advanced Manufacturing Technology 24(3): 241-250.
4. **Feng, G.-H.; Pan, Y.-L.** 2012. Investigation of ball screw preload variation based on dynamic modeling of a preload adjustable feed-drive system and spectrum analysis of ball-nuts sensed vibration signals, Inter-

national Journal of Machine Tools and Manufacture 52(1): 85-96.
http://dx.doi.org/10.1016/j.ijmachtools.2011.09.008.
5. **Varanasi, K.K.; Nayfeh, S. A.** 2004. The Dynamics of lead-screw drives: low-order modeling and experiments, Journal of Dynamic Systems, Measurement and Control 126(2): 388-396.
http://dx.doi.org/10.1115/1.1771690.
6. **Whalley, R.; Ebrahimi, M.; Abdul-Ameer, A.A.** 2005. Hybrid modelling of machine tool axis drives, International Journal of Machine Tools and Manufacture 45(14): 1560-1576.
http://dx.doi.org/10.1016/j.ijmachtools.2005.03.002.
7. **Frey, S.; Dadalau, A.; Verl, A.** 2012. Expedient modeling of ball screw feed drives, Production Engineering 6(2): 205-211.
8. **Vicente, D.; Hecker, R.; Villegas, F.; Flores, G.** 2010. Modeling and vibration mode analysis of a ball screw drive, The International Journal of Advanced Manufacturing Technology, 1-9 p.
9. **Zhou, Y.; Peng, F.Y.; Cao, X.H.** 2011. Parameter sensitivity analysis of axial vibration for lead-screw feed drives with time-varying framework, Mechanika 17(5): 523-528.
http://dx.doi.org/10.5755/j01.mech.17.5.730.
10. **Okwudire, C.E.; Altintas, Y.** 2009. Hybrid Modeling of Ball Screw Drives With Coupled Axial, Torsional, and Lateral Dynamics, Journal of Mechanical Design 131(7): 071002-071009.
http://dx.doi.org/10.1115/1.3125887.
11. **Gu, U.C.;Cheng, C.C.** 2004. Vibration analysis of a high-speed spindle under the action of a moving mass, Journal of Sound and Vibration 278(4-5): 1131-1146.
http://dx.doi.org/10.1016/j.jsv.2003.10.034.
12. THK Corp., Standard ballscrews Catalog No. 003-1EU, in: http://www.thk.ru.
13. **Okwudire, C.;Altintas, Y.** 2009. Minimum tracking error control of flexible ball screw drives using a discrete-time sliding mode controller, Journal of Dynamic Systems, Measurement and Control 131(5): 051006-051012.
http://dx.doi.org/10.1115/1.3155005.
14. **Sepasi, D.; Nagamune, R.; Sassani, F.** 2012. Tracking control of flexible ball screw drives with runout effect and mass variation, Industrial Electronics, IEEE Transactions on 59(2): 1248-1256.

Liang Dong, WenCheng Tang

HIBRIDINIS MODELIAVIMAS IR RUTULINIO RECIRKULIACINIO PASTŪMOS SRAIGTO SISTEMOS STRUKTŪRINĖ DINAMINĖ ANALIZĖ

R e z i u m ė

Norint turėti pilną rutulinio recirkuliacinio pastūmos sraigto struktūrinės dinamikos vaizdą šiame straipsnyje pateiktas hibridinis modeliavimo metodas. Dinaminės rutulinio recirkuliacinio pastūmos sraigto charakteristikos analizuojamos paskirstytųjų parametrų strypui įvertinant ašinę, sukimo ir lenkimo dinamiką. Dinaminė besisukančio sraigto žadinamo ašine kryptimi lygtis su apibendrintomis ribinėmis sąlygomis sudaryta Lagranžo priartėjimu. Lyginant su eksperimento rezultatais modelis gali tiksliai įvertinti rutulinio recirkuliacinio pastūmos sraigto struktūrinę dinamiką. Tokių parametrų, kaip stalo masė, sraigto žingsnis, stalo padėtis ir struktūrinės dinamikos išankstinė rutulinio recirkuliacinio sraigto apkrova yra aptariama. Galiausiai hibridinis modelis yra integruotas į servo valdymo sistemą, kuri sudaro integruotą galimo servo mechanizmo brėžinį.

Liang Dong, WenCheng Tang

HYBRID MODELING AND ANALYSIS OF STRUCTURAL DYNAMIC OF A BALL SCREW FEED DRIVE SYSTEM

S u m m a r y

In order to get the complete structural dynamic of the ball screw drive this paper proposes a hybrid modeling method. The dynamic characteristic of a ball screw is analyzed by a continuous beam approach having axial, torsional and flexural dynamics. The dynamic equation of a rotating screw subjected to the axially moving load with general boundary conditions are obtained through Lagrangian approach. Compared with the experimental results, the model can accurately capture the structural dynamics of the ball screw drive. Influences of parameters, such as table mass, screw pitch, table position and preload on the structural dynamic of the ball screw drive are discussed. Finally, the hybrid model is integrated into a servo control system, which makes an integrated design of the servo-mechanisms possible.

Key words: ball screw, feed drive, vibration, hybrid model, moving load.

Received January 06, 2012
Accepted June 03, 2013